PHYSICAL REVIEW D **81,** 063533 (2010)

Non-Gaussianity in the foreground-reduced CMB maps

A. Bernui[1,2,*] and M. J. Rebouças[1,†]

[1]*Centro Brasileiro de Pesquisas Físicas, Rua Doctor Xavier Sigaud 150, 22290-180 Rio de Janeiro—RJ, Brazil*
[2]*Instituto de Ciências Exatas, Universidade Federal de Itajubá, 37500-903 Itajubá—MG, Brazil*

(Received 20 November 2009; revised manuscript received 23 February 2010; published 30 March 2010)

A detection or nondetection of primordial non-Gaussianity by using the cosmic microwave background radiation (CMB) data is crucial not only to discriminate inflationary models but also to test alternative scenarios. Non-Gaussianity offers, therefore, a powerful probe of the physics of the primordial Universe. The extraction of primordial non-Gaussianity is a difficult enterprise since several effects of a non-primordial nature can produce non-Gaussianity. Given the far-reaching consequences of such a non-Gaussianity for our understanding of the physics of the early Universe, it is important to employ a range of different statistical tools to quantify and/or constrain its amount in order to have information that may be helpful for identifying its causes. Moreover, different indicators can in principle provide information about distinct forms of non-Gaussianity that can be present in CMB data. Most of the Gaussianity analyses of CMB data have been performed by using part-sky frequency, where the mask is used to deal with the galactic diffuse foreground emission. However, full-sky map seems to be potentially more appropriate to test for Gaussianity of the CMB data. On the other hand, masks can induce bias in some non-Gaussianity analyses. Here we use two recent large-angle non-Gaussianity indicators, based on skewness and kurtosis of large-angle patches of CMB maps, to examine the question of non-Gaussianity in the available full-sky five-year and seven-year Wilkinson Microwave Anisotropy Probe (WMAP) maps. We show that these full-sky foreground-reduced maps present a significant deviation from Gaussianity of different levels, which vary with the foreground-reducing procedures. We also make a Gaussianity analysis of the foreground-reduced five-year and seven-year WMAP maps with a $KQ75$ mask, and compare with the similar analysis performed with the corresponding full-sky foreground-reduced maps. This comparison shows a significant reduction in the levels of non-Gaussianity when the mask is employed, which provides indications on the suitability of the foreground-reduced maps as Gaussian reconstructions of the full-sky CMB.

DOI: 10.1103/PhysRevD.81.063533 PACS numbers: 98.80.Es, 98.70.Vc, 98.80.−k

I. INTRODUCTION

A key prediction of a number of simple single-field slow-roll inflationary models is that they cannot generate detectable non-Gaussianity of the cosmic microwave background (CMB) temperature fluctuations within the level of accuracy of the Wilkinson Microwave Anisotropy Probe (WMAP) [1]. There are, however, several inflationary models that can generate non-Gaussianity at a level detectable by the WMAP. These non-Gaussian scenarios comprise models based upon a wide range of mechanisms, including special features of the inflation potential and violation of one of the following four conditions: single field, slow roll, canonical kinetic energy, and initial Bunch-Davies vacuum state. Thus, although convincing detection of a fairly large primordial non-Gaussianity in the CMB data would not rule out all inflationary models, it would exclude the entire class of stationary models that satisfy simultaneously these four conditions (see, e.g., Refs. [2–4]). Moreover, a null detection of deviation from Gaussianity would rule out alternative models of the early Universe (see, for example, Ref. [5]). Thus, a detection or nondetection of primordial non-Gaussianity in the CMB data is crucial not only to discriminate (or even exclude classes of) inflationary models but also to test alternative scenarios, offering therefore a window into the physics of the primordial Universe.

However, there are various nonprimordial effects that can also produce non-Gaussianity such as, e.g., unsubtracted foreground contamination, unconsidered point sources emission, and systematic errors [6–8]. Thus, the extraction of a possible primordial non-Gaussianity is not a simple endeavor. In view of this, a great deal of effort has recently gone into verifying the existence of non-Gaussianity by employing several statistical estimators [9] (for related articles see, e.g., Ref. [10]). Different indicators can in principle provide information about multiple forms of non-Gaussianity that may be present in WMAP data. It is therefore important to test CMB data for deviations from Gaussianity by using a range of different statistical tools to quantify or constrain the amount of any non-Gaussian signals in the data, and extract information on their possible origins.

A number of recent analyses of CMB data performed with different statistical tools have provided indications of

*bernui@unifei.edu.br
†reboucas@cbpf.br

either consistency or deviation from Gaussianity in the CMB temperature fluctuations (see, e.g., Ref. [9]). In a recent paper [11] we proposed two new large-angle non-Gaussianity indicators, based on skewness and kurtosis of large-angle patches of CMB maps, which provide measures of the departure from Gaussianity on large angular scales. We used these indicators to search for the large-angle deviation from Gaussianity in the three- and five-year single frequency maps with a $KQ75$ mask, and found that while the deviation for the Q, V, and W masked maps is within the 95% expected values of Monte Carlo (MC) statistically Gaussian CMB maps, there is a strong indication of deviation from Gaussianity ($\gg 95\%$ off the MC) in the K and Ka masked maps.

Most of the Gaussianity analyses with WMAP data have been carried out by using CMB temperature fluctuation maps (raw and clean) in the frequency bands Q, V, and W or some combination of these maps. In these analyses, in order to deal with the diffuse galactic foreground emission, masks such as, for example, $KQ75$ and $Kp0$ have been used.

However, sky cuts themselves can potentially induce bias in Gaussianity analyses, and on the other hand full-sky maps seem more appropriate to test for Gaussianity in the CMB data. Thus, a pertinent question that arises is how the analysis of Gaussianity in Ref. [11] is modified if whole-sky foreground-reduced CMB maps are used. Our primary objective in this paper is to address this question by extending the analysis of Ref. [11] in three different ways. First, we use the same statistical indicators to carry out a new analysis of Gaussianity of the available full-sky foreground-reduced five-year and seven-year CMB maps [12–15]. Second, since in these maps the foreground is reduced through different procedures each of the resulting maps should be tested for Gaussianity. Thus, we make a quantitative analysis of the effects of distinct cleaning processes in the deviation from Gaussianity, quantifying the level of non-Gaussianity for each foreground reduction method. Third, we study quantitatively the consequences for the Gaussianity analysis of masking the foreground-reduced maps with the $KQ75$ mask. An interesting outcome is that this mask lowers significantly the level of deviation from Gaussianity even in the foreground-reduced maps, rendering therefore information about the suitability of the foreground-reduced maps as Gaussian reconstructions of the full-sky CMB.

II. NON-GAUSSIANITY INDICATORS

The chief idea behind our construction of the non-Gaussianity indicators is that a simple way of accessing the deviation from Gaussianity distribution of the CMB temperature fluctuations is by calculating the skewness $S = \mu_3/\sigma^3$ and the kurtosis $K = \mu_4/\sigma^4 - 3$ from the fluctuations data, where μ_3 and μ_4 are the third and fourth central moments of the distribution and σ is its variance. Clearly calculating S and K from the whole-sky temperature fluctuations data would simply yield two dimensionless numbers, which are rough measures of deviation from Gaussianity of the temperature fluctuation distribution.

However, one can go further and obtain a great number of values associated to directional information of deviation from Gaussianity if instead one takes a discrete set of points $\{j = 1, \ldots, N_c\}$ homogeneously distributed on the celestial sphere S^2 as the center of spherical caps of a given aperture γ and calculate S_j and K_j from the CMB temperature fluctuations of each spherical cap. The values S_j and K_j can then be taken as measures of the non-Gaussianity in the direction (θ_j, ϕ_j) of the center of the spherical cap j. Such calculations for the individual caps thus provide quantitative information ($2N_c$ values) about possible violation of Gaussianity in the CMB data.

This procedure is a constructive way of defining two discrete functions S and K (defined on S^2) from the temperature fluctuations data, and can be formalized through the following steps (for more details, see Ref. [11]):

(i) Take a discrete set of points $\{j = 1, \ldots, N_c\}$ homogeneously distributed on the CMB celestial sphere S^2 as the centers of spherical caps of a given aperture γ.

(ii) Calculate for each spherical cap j the skewness (S_j) and kurtosis (K_j) given, respectively, by

$$S_j = \frac{1}{N_p \sigma_j^3} \sum_{i=1}^{N_p} (T_i - \bar{T}_j)^3, \tag{1}$$

and

$$K_j = \frac{1}{N_p \sigma_j^4} \sum_{i=1}^{N_p} (T_i - \bar{T}_j)^4 - 3, \tag{2}$$

where N_p is the number of pixels in the jth cap, T_i is the temperature at the ith pixel, $\bar{T}_j$ is the CMB mean temperature in the jth cap, and σ is the standard deviation. Clearly, the values S_j and K_j obtained in this way for each cap can be viewed as a measure of non-Gaussianity in the direction of the center of the cap (θ_j, ϕ_j).

(iii) Patching together the S_j and K_j values for each spherical cap, one obtains our indicators, i.e., discrete functions $S = S(\theta, \phi)$ and $K = K(\theta, \phi)$ defined over the celestial sphere, which can be used to measure the deviation from Gaussianity as a function of the angular coordinates (θ, ϕ). The Mollweid projection of skewness and kurtosis functions $S = S(\theta, \phi)$ and $K = K(\theta, \phi)$ are nothing but skewness and kurtosis maps; hereafter we shall refer to them as S map and K map, respectively.

Now, since $S = S(\theta, \phi)$ and $K = K(\theta, \phi)$ are functions defined on S^2 they can be expanded into their spherical harmonics in order to have their power spectra S_l and K_l.

Thus, for example, for the skewness indicator $S = S(\theta, \phi)$ one has

$$S(\theta, \phi) = \sum_{l=0}^{\infty} \sum_{m=-l}^{l} b_{lm} Y_{lm}(\theta, \phi), \tag{3}$$

and can calculate the corresponding angular power spectrum

$$S_l = \frac{1}{2l+1} \sum_m |b_{lm}|^2, \tag{4}$$

which can be used to quantify the angular scale of the deviation from Gaussianity, and also to calculate the statistical significance of such deviation. Obviously, similar expressions hold for the kurtosis $K = K(\theta, \phi)$.

In the next section we shall use the statistical indicators $S = S(\theta, \phi)$ and $K = K(\theta, \phi)$ to test, for Gaussianity, the available foreground-reduced maps obtained from the five-year WMAP data.

III. NON-GAUSSIANITY

A. Foregound-reduced maps

The WMAP team has released high angular resolution five-year maps of the CMB temperature fluctuations in the five frequency bands K (22.8 GHz), Ka(33.0 GHz), Q (40.7 GHz), V (60.8 GHz), and W (93.5 GHz). It has also produced a full-sky foreground-reduced internal linear combination (ILC) map which is formed from a weighted linear combination of these five frequency band maps in which the weights are chosen in order to minimize the galactic foreground contribution.

It is well known that the first-year ILC map is inappropriate for CMB scientific studies [16]. However, in the five-year (also in the three-year and seven-year) version of this map a bias correction has been implemented as part of the foreground cleaning process, and the WMAP team suggested that this map is suitable for use in large angular scales (low l) analyses, although the WMAP team admittedly has not performed non-Gaussian tests on this version of the ILC map [12,17]. Notwithstanding the many merits of the five-year ILC procedure, some cleaning features of this ILC approach have been considered, and two variants have been proposed recently. In the first approach the frequency dependent weights were determined in harmonic space [13], while in the second the foreground is reduced by using needlets as the basis of the cleaning process [14]. Thus, two new full-sky foreground-cleaned maps have been produced with the WMAP five-year data, namely, the harmonic ILC (HILC) [13] and the needlet ILC (NILC) (for more details see Refs. [13,14]).

In the next section, we use the full-sky foreground-reduced ILC, HILC, and NILC maps with the same smoothed 1° resolution (which is the resolution of the ILC map) as the input maps from which we calculate the $S = S(\theta, \phi)$ and $K = K(\theta, \phi)$ maps, and then we compute the associated power spectra in order to carry out a statistical analysis to quantify the levels of deviation from Gaussianity.[1]

B. Analysis and results

In order to minimize the statistical noise, in the calculations of skewness and kurtosis maps (S map and K map) from the foreground-reduced maps, we have scanned the celestial sphere with spherical caps of aperture $\gamma = 90°$, centered at 12 288 points homogeneously generated on the two-sphere by using the HEALPIX code [19]. In other words, the point centers of the spherical caps are the center of the pixels of a homogeneous pixelization of the S^2 generated by HEALPIX with $N_{\rm side} = 32$. We emphasize, however, that this pixelization is only a practical way of choosing the centers of the caps homogeneously distributed on S^2. It is not related to the pixelization of the above-mentioned ILC, HILC, and NILC input maps that we have utilized to calculate both the S and K maps from which we compute the associated power spectra.

Figures 1 and 2 show examples of S and K maps obtained from the foreground-reduced NILC full-sky and $KQ75$ maps. The panels of these figures clearly show regions with higher and lower values (''hot'' and ''cold'' spots) of $S(\theta, \phi)$ and $K(\theta, \phi)$, which suggest large-angle multipole components of non-Gaussianity. We have also calculated similar maps (with and without the $KQ75$ mask) from the ILC and HILC maps. However, since these maps provide only qualitative information, to avoid repetition we only depict the maps of Figs. 1 and 2 merely for illustrative purpose.

In order to obtain quantitative information about the large angular scale (low l) distributions for the non-Gaussianity S and K maps obtained from the available full-sky foreground-reduced five-year maps, we have calculated the (low l) power spectra S_l and K_l for these maps. The statistical significance of these power spectra is estimated by comparing with the corresponding multipole values of the averaged power spectra $\bar{S}_l$ and $\bar{K}_l$ calculated from maps obtained by averaging over 1000 Monte Carlo–generated statistically Gaussian CMB maps.[2] Throughout the paper the mean quantities are denoted by overline.

Before proceeding to a statistical analysis, let us describe with some detail our calculations. For the sake of brevity, we focus on the skewness indicator S, but a completely similar procedure was used for the kurtosis indicator K. We generated 1000 MC Gaussian (scrambled) CMB maps, which are then used to generate 1000 skewness S maps, from which we calculate 1000 power spectra: $\{S_l^{\mathbf{i}}\}$ ($\mathbf{i} = 1, \cdots, 1000$ is an enumeration index, and $l = 1, \cdots, 10$).

[1]The ILC, HILC, and NILC maps are available for download. See [18].

[2]Each Monte Carlo scrambled map is a stochastic realization of the WMAP best-fitting angular power spectrum of the ΛCDM model, obtained by randomizing the temperature components a_{lm} within the cosmic variance limits.

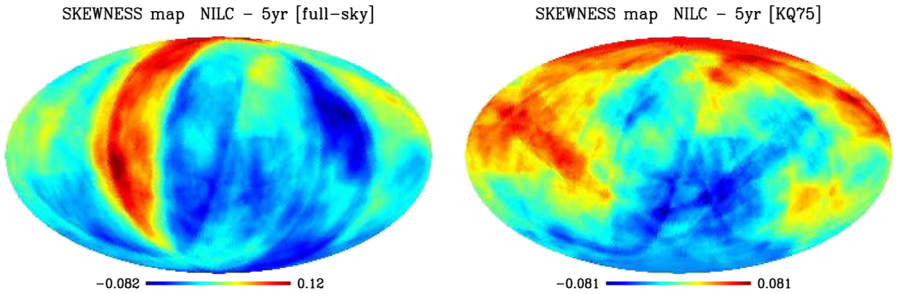

FIG. 1 (color online). Skewness indicator maps calculated from the five-year foreground-reduced NILC full-sky (left panel) and $KQ75$ masked (right panel) maps.

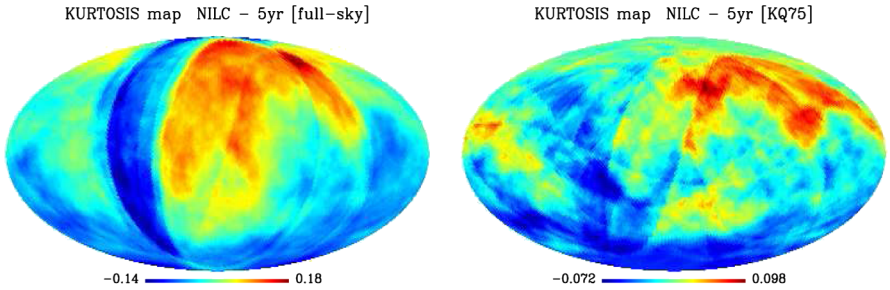

FIG. 2 (color online). Kurtosis indicator maps calculated from the five-year foreground-reduced NILC full-sky (left panel) and $KQ75$ masked (right panel) maps.

In this way, for each fixed multipole component $S^{\mathbf{i}}_{l=\text{fixed}}$ we have 1000 multipole values from which we calculate the mean value $\bar{S}_l = (1/1000)\sum_{\mathbf{i}=1}^{1000} S^{\mathbf{i}}_l$. From this MC process we have at the end ten mean multipole values $\bar{S}_l$, each of which are then used for a comparison with the corresponding multipole values S_l (obtained from the input map) in order to evaluate the statistical significance of the multipole components S_l. To make this comparison easier, instead of using the angular power spectra S_l and K_l themselves, we employed the differential power spectra $|S_l - \bar{S}_l|$ and $|K_l - \bar{K}_l|$, which measure the deviation of the skewness and kurtosis multipole values (calculated from the foreground-reduced maps) from the mean multipoles $\bar{S}_l$ and $\bar{K}_l$ (calculated from the Gaussian maps). Thus, for example, to study the statistical significance of the quadrupole component of the skewness from HILC map S_2^{HILC} (say) we calculate the deviation $|S_2^{\text{HILC}} - \bar{S}_2|$, where the mean quadrupole value $\bar{S}_2$ is calculated from the $\mathbf{i} = 1, \cdots, 1000$ quadrupole values of the MC Gaussian maps.

Figure 3 shows the differential power spectra calculated from full-sky five-year foreground-reduced maps; i.e., it displays the absolute value of the deviations from the mean angular power spectrum of the skewness S_l (left panel) and kurtosis K_l (right panel) indicators for $l = 1, \cdots, 10$, which is a range of multipole values needed to investigate the large-scale angular characteristics of the S and K maps. This figure shows a first indication of deviation from Gaussianity in five-year foreground-reduced ILC, HILC, and NILC maps in that the deviations $|S_l - \bar{S}_l|$ and $|K_l - \bar{K}_l|$ for these maps are not within 95% of the mean MC value.

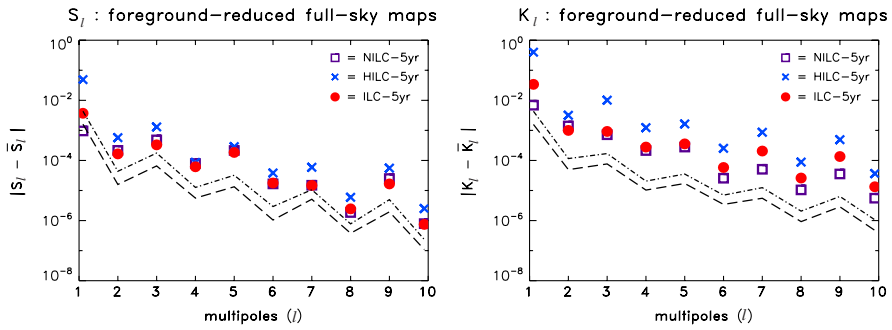

FIG. 3 (color online). Differential power spectrum of skewness $|S_l - \bar{S}_l|$ (left) and kurtosis $|K_l - \bar{K}_l|$ (right) indicators calculated from the full-sky foreground-reduced ILC, HILC, and NILC maps obtained from the WMAP five-year data. The 68% and 95% confidence levels are indicated, respectively, by the dashed and dash-dotted lines.

To obtain additional quantitative information regarding the deviation from Gaussianity, we can also calculate the percentage of the deviations $|S_l^{\mathbf{i}} - \bar{S}_l|$ calculated from 1000 MC Gaussian maps, which are smaller than $|S_l - \bar{S}_l|$ obtained from each foreground-reduced map. This calculations are made in detail in Appendix A. Thus, for example, we have for the full-sky NILC, HILC, and ILC maps, respectively, that ~99.999%, ~99.999%, and 99.900% of the multipole values $S_5^{\mathbf{i}}$ obtained from the MC maps are closer to the mean $\bar{S}_5$ than the value S_5 calculated from the data, i.e., from each of the foreground-reduced maps. This indicates how unlikely are the occurrences of the values obtained from these foreground-reduced maps for the multipole S_5 in the set of values of $S_5^{\mathbf{i}}$ from MC simulated maps. In other words, the probability of occurrence of the S_5 values (in the set of MC values) for the NILC, HILC, and ILC maps is only $\mathcal{O}(10^{-3})\%$, $\mathcal{O}(10^{-3})\%$, and $\mathcal{O}(10^{-1})\%$, respectively. Similarly, the probability of occurrence of K_2, for example, is $\mathcal{O}(10^{-3})\%$ for all these foreground-reduced maps, while for K_5 is, respectively, $\mathcal{O}(10^{-1})\%$ (NILC), $\mathcal{O}(10^{-3})\%$ (HILC), and $\mathcal{O}(10^{-3})\%$ (ILC). In Tables IV and VI of Appendix A we collect together the probability of occurrence of each of the values S_l and K_l ($l = 1, \cdots, 10$) calculated from S and K maps obtained from the full-sky NILC, HILC, and ILC maps. In Tables V and VII we present these probabilities calculated from the same input maps but now with the $KQ75$ mask.[3] The comparison of Table IV with Table V, and of Table VI with Table VII, makes apparent the role of the $KQ75$ mask in reducing the level of deviation from Gaussianity (see Appendix A for more details).

Although the set of "local" (fixed l) estimates collected together in the tables of Appendix A gives an indication of deviation from Gaussianity as measured by each multipole component to have an overall assessment of low l power spectra S_l and K_l calculated from each CMB foreground-reduced map, we have performed a χ^2 test to find out the goodness of fit for S_l and K_l multipole values as compared to the expected multipole values from the MC Gaussian maps. In this way, we can obtain one number for each foreground-reduced map that collectively ("globally") quantifies the deviation from Gaussianity. For the power spectra S_l and K_l we found the values given in Table I for the ratio χ^2/dof (dof stands for degrees of freedom) for the power spectra calculated from HILC, ILC, and NILC full-sky input maps. Clearly a good fit occurs when $\chi^2/\text{dof} \sim 1$. Moreover, the greater the χ^2/dof values, the smaller the χ^2 probabilities, that is, the probability that the multipole values S_l and K_l and the expected MC multipole values agree. Thus, regarding the skewness indicator Table I shows that the HILC presents the greatest level of deviation from Gaussianity ($\chi^2/\text{dof} \gg 1$), as captured by the indicator S, while the NILC map has the lowest level.

TABLE I. Results of the χ^2 test to determine the goodness of fit for S_l and K_l multipole values calculated from the full-sky foreground-reduced HILC, ILC, and NILC maps as compared to the expected multipoles' values from the Gaussian MC maps.

	χ^2 for S_l	χ^2 for K_l
HILC	4625	301 665
ILC	35.7	2368
NILC	7.1	160.3

Regarding the deviation from Gaussianity as detected by the kurtosis indicator K, Table I shows again that the HILC presents the largest deviation followed by the ILC and NILC. To the extent that χ^2/dof is considerably greater than one, all these full-sky foreground-reduced maps also present a significant deviation from Gaussianity as captured here by the kurtosis indicator.

The above results of our statistical analysis given in Fig. 3 and gathered together in Table I (and also supported by Table V of Appendix A) show a significant deviation from Gaussianity in five-year full-sky foreground-reduced (ILC, NILC, and HILC) maps as detected by both the skewness and the kurtosis indicators S and K. A pertinent question that arises here is how this analysis of Gaussianity for the full-sky foreground-reduced maps is modified if one uses the $KQ75$ mask, which was recommended by the WMAP team for tests of Gaussianity of the five-year band maps. Furthermore, the combination of the full-sky and mask analyses should provide information on the reliability of the foreground-reduced maps as appropriate reconstructions of the full-sky CMB.

Figure 4 shows the power spectra $|S_l - \bar{S}_l|$ (left) and $|K_l - \bar{K}_l|$ (right) calculated from five-year foreground-reduced $KQ75$ masked maps. This figure along with Fig. 3 show a significant reduction in the level of deviation from Gaussianity when the foreground-reduced ILC, HILC, and NILC maps are masked. To quantify this reduction we have recalculated χ^2/dof for these input maps with the $KQ75$ mask, and have collected the results in Table II. The comparison of Tables I and II shows quantitatively the reduction of the level of Gaussianity for the case of CMB masked maps.[4]

[3]We emphasize that, throughout this paper, in the implementation of the mask we do not take $T = 0$ for the temperature fluctuation of the pixels inside the masked region. This would clearly induce a non-Gaussian contribution. In our scan of the CMB sky when the spherical cap moves into the masked area, the pixels of the cap inside the masked area do not contribute to the values of the indicators in the center of the cap. In these cases the values S_j and K_j for a jth cap are calculated with a small number N_p of pixels.

[4]Incidentally, this reduction is also revealed through (and agrees with) the comparison of Table IV with Table V, and of Table VI with Table VII.

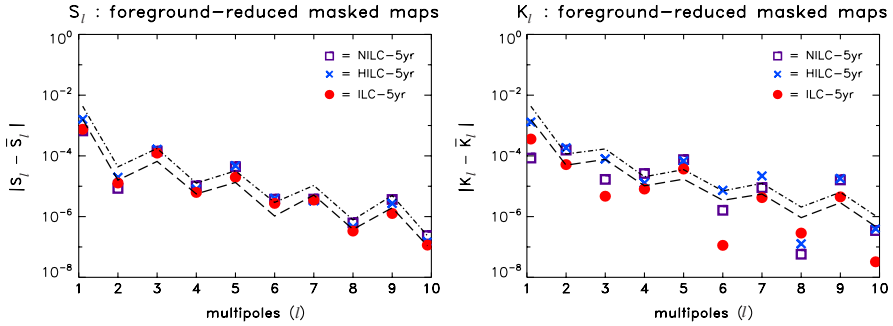

FIG. 4 (color online). Differential power spectrum of skewness $|S_l - \bar{S}_l|$ (left) and kurtosis $|K_l - \bar{K}_l|$ (right) indicators calculated from the five-year foreground-reduced $KQ75$ masked ILC, HILC and NILC maps. The 68% and 95% confidence levels are indicated, respectively, by the dashed and dash-dotted lines.

In the above analyses we have followed the five-year WMAP recommendation for tests of Gaussianity and thus used the mask $KQ75$, which is slightly more conservative than the $Kp0$ (the $KQ75$ sky cut is 28.4%, while the $Kp0$ cut is 24.5%). A pertinent question at this point is how the above results are modified if the less conservative $Kp0$ mask is used. We have examined this issue by calculating the power spectra S_l and K_l and the χ^2/dof from S and K maps obtained from the ILC, NILC, and HILC input maps with the $Kp0$ mask. The result of this analysis is given in Table III.

A comparison between Tables II and III shows that in general the value of χ^2/dof increases for both indicators when the less conservative mask $Kp0$ is used. We note that the changes in χ^2/dof values are greater for the HILC, though.

The comparison between Figs. 3 and 4, and Tables I and II along with the tables of Appendix A, clearly provides quantitative information on the suitability of the foreground-reduced maps as Gaussian reconstructions of the full-sky CMB, and makes apparent the relevant role of the mask $KQ75$ in reducing significantly the level of non-Gaussianity in these foreground-reduced maps.

TABLE II. Results of the χ^2 test to determine the goodness of fit for S_l and K_l multipole values calculated from the foreground-reduced HILC, ILC, and NILC maps with a $KQ75$ mask as compared to the expected multipoles' values from the Gaussian MC masked maps.

	χ^2 for S_l $[KQ75]$	χ^2 for K_l $[KQ75]$
HILC	4.7	4.2
ILC	1.2	0.4
NILC	1.4	1.1

TABLE III. Results of the χ^2 test to determine the goodness of fit for S_l and K_l multipole values calculated from the S and K maps obtained from the foreground-reduced HILC, ILC, and NILC maps with a $Kp0$ mask as compared to the expected multipoles' values from the Gaussian MC masked maps.

	χ^2 for S_l $[Kp0]$	χ^2 for K_l $[Kp0]$
HILC	58.7	101.9
ILC	1.9	6.5
NILC	4.5	17.9

The calculations of our non-Gaussianity indicators require the specification of some quantities whose choice could in principle affect the outcome of our calculations. To test the robustness of our scheme, hence of our results, we studied the effects of changing in the parameters employed in the calculation of our indicators. We found that the S and K angular power spectra do not change appreciably as we change the resolution of CMB temperature maps used and the number of point centers of the caps with values 768, 3072, and 12 288 (see Ref. [11] for more details on the robustness of this method).

Concerning the robustness of the above analyses with the $KQ75$ mask, some additional words of clarification are in order here. First, we note that the calculations of the S maps and K maps by scanning the CMB masked maps sometimes include caps whose center is within or close to the $KQ75$ masked region. In these cases, the calculations of the S and K indicators are made with a smaller number of pixels, which clearly introduce additional statistical noise as compared to the full-sky map cases. In order to minimize this effect we have scanned the CMB masked sky with spherical caps of aperture $\gamma = 90°$, and for the sake of uniformity we have used caps with the same aperture for the full-sky maps. We note, however, that full-sky foreground-reduced analysis does not change significantly if one uses smaller apertures such as, for example, $\gamma \simeq 60°$.

IV. CONCLUDING REMARKS

The detection or nondetection of primordial non-Gaussianity in the CMB data is essential to discriminate or even exclude classes of inflationary models. It can also be used to test alternative scenarios of the primordial Universe. There are, however, several nonprimordial effects that can also produce non-Gaussianity. This makes the extraction of a possible primordial non-Gaussianity a

rather difficult endeavor. Since different indicators can in principle provide information about distinct forms of non-Gaussianity, it is important to test CMB data for non-Gaussianity by using different estimators to quantify and/or constrain its amount in order to extract information about their possible sources.

Most of the Gaussianity analyses of CMB data have been performed with frequency band maps. In these studies, to deal with the galactic diffuse foreground emission, masks have been employed. However, a full-sky foreground-reduced map seems to be potentially more appropriate to test the CMB data for Gaussianity.[5] The five-year version of the ILC map has been suggested as a full-sky map suitable for large angular scales analyses [17], even though the WMAP team has not performed a battery of non-Gaussianity tests on this map [12].

In this paper we have performed an analysis of Gaussianity of the available five-year full-sky foreground-reduced maps. To this end, we have used two new non-Gaussianity indicators based on skewness and kurtosis of large-angle patches of CMB maps, which provide a measure of departure from Gaussianity on large angular scales [11]. We have shown that the full-sky five-year foreground-reduced maps (ILC, HILC, and NILC) present a significant deviation from Gaussianity, which varies with the foreground-reducing procedures. We have established which of these full-sky foreground-reduced maps exhibit the highest and the lowest level of non-Gaussianity.

We have also masked the foreground-reduced maps with $KQ75$ and $Kp0$ masks and performed a quantitative analysis of deviation from Gaussianity of these maps. The comparison of the full-sky and masked analyses (see Figs. 3 and 4 and Tables I, II, and III) shows a significant reduction in the levels of non-Gaussianity when the masks are employed, which in turn provides indications on the suitability of the foreground-reduced maps as Gaussian reconstructions of the full-sky CMB.

Finally, when we were in the process of rewriting a revised version of this paper, by taking into account the referee's recommendations, the seven-year WMAP CMB data were released, including a new version of the full-sky foreground-reduced ILC map [15]. We have considered this latest foreground-reduced ILC map, and performed a complete additional analysis of the Gaussianity of the five- and seven-year versions of the ILC maps, whose details are given in Appendix B.[6] The main result of this appendix is that the full-sky seven-year foreground-reduced ILC map also presents a significant deviation from Gaussianity, which again is reduced substantially when the $KQ75$ mask is employed. In this way, our results are robust with respect to seven-year WMAP CMB data.

[5]In reality, the full-sky map seems to be the most suitable for a number of other issues, including the test of statistical isotropy, the search for evidence of a North-South asymmetry in CMB data, and signatures of a possible nontrivial cosmic topology, for example.

[6]Note that there are no available seven-year HILC and NILC maps.

ACKNOWLEDGMENTS

This work is supported by Conselho Nacional de Desenvolvimento Científico e Tecnológico (CNPq)—Brasil, under Grant No. 472436/2007-4. M. J. R. and A. B. thank CNPq for the grants under which this work was carried out. We are also grateful to A. F. F. Teixeira for reading the manuscript and indicating the omissions and misprints. We acknowledge the use of the Legacy Archive for Microwave Background Data Analysis (LAMBDA). Some of the results in this paper were derived using the HEALPIX package [19].

APPENDIX A

Clearly from 1000 MC maps one can calculate for each l one thousand values of both $S_l^{\mathbf{i}}$ and $K_l^{\mathbf{i}}$ ($\mathbf{i} = 1, \cdots, 1000$) and the corresponding mean values $\bar{S}_l$ and $\bar{K}_l$. For the sake of brevity in what follows we focus on the skewness indicator S, but completely similar calculations were used to have the probabilities for kurtosis indicator K.

With the MC values $S_l^{\mathbf{i}}$ and the mean $\bar{S}_l$ one can calculate the percentages of values of the deviations $|S_l^{\mathbf{i}} - \bar{S}_l|$ calculated from 1000 MC Gaussian maps which are smaller than $|S_l - \bar{S}_l|$ with S_l obtained from the data (full-sky and masked maps). For each multipole this number indicates how unlikely are the occurrences of the values obtained from the data (input maps) for that multipole in the set of values $\{S_l^{\mathbf{i}}\}$ obtained from MC Gaussian maps. In this way one can calculate the probability of occurrence of a given multipole value S_l (obtained from the data) in the set of MC values (obtained from the MC maps) for each

TABLE IV. The probability (percentage) of occurrence of the multipole values S_l calculated from the data in the set $\{S_l^{\mathbf{i}}\}$ of values computed from MC Gaussian CMB maps. The data from the five-year full-sky foreground-reduced NILC, HILC, and ILC maps were used.

l	NILC [full-sky]	HILC [full-sky]	ILC [full-sky]
1	51.7%	$\mathcal{O}(10^{-3})$%	3.7%
2	$\mathcal{O}(10^{-3})$%	$\mathcal{O}(10^{-3})$%	$\mathcal{O}(10^{-3})$%
3	0.1%	0.1%	0.4%
4	$\mathcal{O}(10^{-3})$%	$\mathcal{O}(10^{-3})$%	0.1%
5	$\mathcal{O}(10^{-3})$%	$\mathcal{O}(10^{-3})$%	0.1%
6	$\mathcal{O}(10^{-3})$%	$\mathcal{O}(10^{-3})$%	$\mathcal{O}(10^{-3})$%
7	1.2%	0.1%	1.3%
8	0.1%	0.1%	0.1%
9	$\mathcal{O}(10^{-3})$%	$\mathcal{O}(10^{-3})$%	$\mathcal{O}(10^{-3})$%
10	0.1%	$\mathcal{O}(10^{-3})$%	0.1%

TABLE V. The probability (percentage) of occurrence of multipole values S_l calculated from the data in the set $\{S_l^{\mathrm{i}}\}$ of values computed from MC Gaussian CMB maps. The data from the five-year NILC, HILC, and ILC $KQ75$ masked maps were used.

l	NILC [$KQ75$]	HILC [$KQ75$]	ILC [$KQ75$]
1	76.7%	34.1%	73.7%
2	69.1%	12.8%	42.1%
3	4.6%	3.7%	5.7%
4	7.2%	8.9%	16.3%
5	2.7%	2.2%	11.3%
6	2.4%	1.5%	4.0%
7	51.4%	57.6%	54.1%
8	4.9%	10.2%	40.6%
9	7.0%	13.8%	55.0%
10	3.9%	8.4%	27.7%

foreground-reduced CMB map. In Tables IV, V, VI, and VII we collect together the results of such calculations.

Thus, for example, from Table IV we have for the full-sky NILC, HILC, and ILC maps, respectively, the probability of occurrence of the S_6 values (in the set of MC values) is $\mathcal{O}(10^{-3})\%$, whereas from Table VI the probability for K_6 is, respectively, 0.1%, $\mathcal{O}(10^{-3})\%$, and 0.1% for the full-sky NILC, HILC, and ILC input maps.

The comparison of Table IV with Table V, and of Table VI with Table VII, shows that the role of the $KQ75$ mask is to cut down significantly the level of deviation from Gaussianity for all multipoles S_l and K_l obtained from the foreground-reduced input maps. This is clear because the probabilities of occurrences for these multipoles' values in the set of MC multipole values increase substantially when the mask is employed.

Although the estimates of probabilities collected in these tables give a clear quantitative indication of deviation from Gaussianity, an overall assessment of the power spectra S_l and K_l can be obtained through the χ^2 test of the goodness

TABLE VI. The probability (percentage) of occurrence of the multipole values K_l calculated from the data in the set $\{K_l^{\mathrm{i}}\}$ of values computed from MC Gaussian CMB maps. The data from the five-year full-sky foreground-reduced NILC, HILC, and ILC maps were utilized.

l	NILC [full-sky]	HILC [full-sky]	ILC [full-sky]
1	0.6%	$\mathcal{O}(10^{-3})\%$	$\mathcal{O}(10^{-3})\%$
2	$\mathcal{O}(10^{-3})\%$	$\mathcal{O}(10^{-3})\%$	$\mathcal{O}(10^{-3})\%$
3	0.1%	$\mathcal{O}(10^{-3})\%$	0.1%
4	$\mathcal{O}(10^{-3})\%$	$\mathcal{O}(10^{-3})\%$	$\mathcal{O}(10^{-3})\%$
5	0.1%	$\mathcal{O}(10^{-3})\%$	$\mathcal{O}(10^{-3})\%$
6	0.1%	$\mathcal{O}(10^{-3})\%$	0.1%
7	0.4%	$\mathcal{O}(10^{-3})\%$	$\mathcal{O}(10^{-3})\%$
8	0.1%	$\mathcal{O}(10^{-3})\%$	$\mathcal{O}(10^{-3})\%$
9	0.1%	$\mathcal{O}(10^{-3})\%$	$\mathcal{O}(10^{-3})\%$
10	0.1%	$\mathcal{O}(10^{-3})\%$	$\mathcal{O}(10^{-3})\%$

TABLE VII. The probability (percentage) of occurrence of the multipole value K_l calculated from the data in the set $\{K_l^{\mathrm{i}}\}$ of values computed from MC Gaussian CMB maps. The data from the five-year foreground-reduced NILC, HILC, and ILC $KQ75$ masked maps were employed.

l	NILC [$KQ75$]	HILC [$KQ75$]	ILC [$KQ75$]
1	87.0%	45.1%	81.1%
2	2.3%	1.9%	23.6%
3	85.6%	29.3%	89.1%
4	2.3%	9.0%	57.1%
5	1.3%	1.8%	4.7%
6	82.6%	4.2%	98.1%
7	8.8%	1.7%	46.9%
8	96.6%	93.2%	86.6%
9	0.9%	0.8%	5.0%
10	65.0%	54.2%	97.7%

of fit for S_l and K_l from the data as compared to the expected multipoles' values obtained from the Gaussian MC maps. This point is discussed in Sec. III B.

APPENDIX B

While we were in the final phase of writing a modified version of this paper, a new version of the full-sky foreground-reduced ILC map was released by the WMAP team [15]. Since there is no available version of the NILC and HILC maps obtained from the seven-year WMAP data to be considered, here we present the results of a comparative analysis of deviation from Gaussianity performed by using the five- and seven-year versions of the ILC as input maps. As the calculations are similar to those of Sec. III B we refer the readers to that section for more details.

Figure 5 shows the differential power spectra calculated from the full-sky five- and seven-year foreground-reduced ILC input maps (ILC5 and ILC7, for short). Apart from some local deviation of the deviations $|S_l - \bar{S}_l|$ and $|K_l - \bar{K}_l|$, this figure shows a deviation from Gaussianity, which is quantified in Table VIII.

It is interesting to note that the deviation from Gaussianity as measured by our indicators is greater for the ILC7 than for the ILC5 input map. Concerning this point some words of clarification are in order here. First, we note that the details of the algorithm used to compute the ILC7 maps are the same as those of the ILC5 map. However, to take into account the most recent updates to the calibration and beams, the frequency weights for each of the 12 regions (in which the sky is subdivided in the ILC method) are slightly different in the calculation of the ILC7 map. Second, the difference between the ILC7 and ILC5 maps is a map whose small-scale differences are consistent with the pixel noise, but with a large-scale dipolar component, with the large-scale differences being consistent with a change in dipole of $6.7\mu K$ [15]. Thus, the resultant ILC7

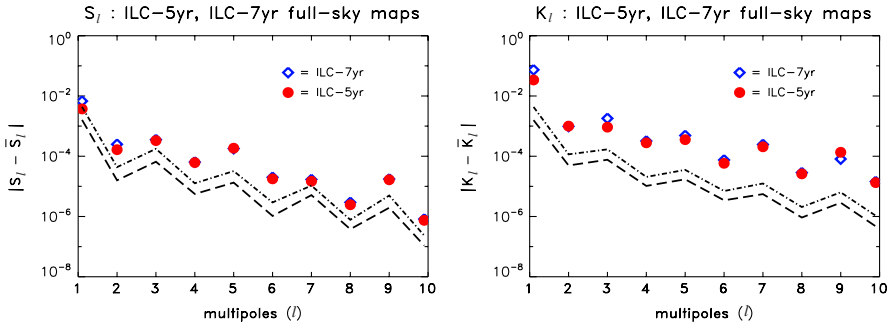

FIG. 5 (color online). Differential power spectrum of skewness $|S_l - \bar{S}_l|$ (left) and kurtosis $|K_l - \bar{K}_l|$ (right) indicators calculated from the full-sky foreground-reduced ILC input map obtained from the WMAP five-year and seven-year data. The 68% and 95% confidence levels are indicated, respectively, by the dashed and dash-dotted lines.

TABLE VIII. Results of the χ^2 test to determine the goodness of fit for S_l and K_l multipole values calculated from the foreground-reduced ILC5 and ILC7 full-sky maps as compared to the expected multipoles' values from the MC Gaussian full-sky maps.

	χ^2 for S_l [full-sky]	χ^2 for K_l [full-sky]
ILC5	35.7	2368
ILC7	103	10 507

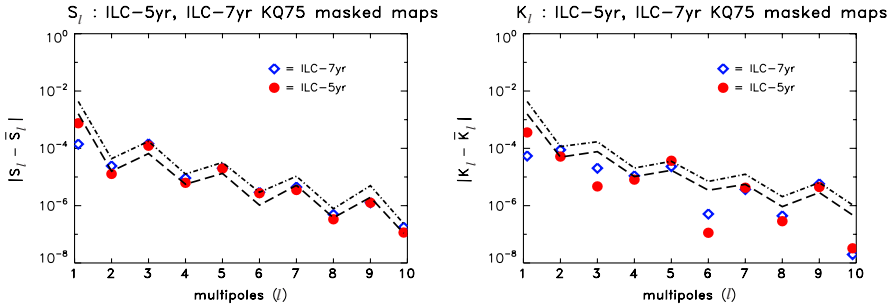

FIG. 6 (color online). Differential power spectrum of skewness $|S_l - \bar{S}_l|$ (left) and kurtosis $|K_l - \bar{K}_l|$ (right) indicators calculated from the five-year and seven-year foreground-reduced ILC input maps with a $KQ75$ mask. The 68% and 95% confidence levels are indicated, respectively, by the dashed and dash-dotted lines.

TABLE IX. Results of the χ^2 test to determine the goodness of fit for S_l and K_l multipole values calculated from the foreground-reduced ILC5 and ILC7 maps with a $KQ75$ mask as compared to the expected multipoles' values from the Gaussian MC masked maps.

	χ^2 for S_l [$KQ75$]	χ^2 for K_l [$KQ75$]
ILC5	1.2	0.4
ILC7	0.7	0.2

map is not indistinguishable from the ILC5 map, and the differences between them have been captured by our indicators.

Figure 6 shows the differential power spectra calculated from a five-year and seven-year version of the foreground-reduced ILC maps with a $KQ75$ mask. This figure along with Fig. 5 shows a significant reduction in the level of deviation from Gaussianity when both ILC5 and ILC7 are masked. To quantify this reduction we have calculated χ^2/dof for these input maps with the $KQ75$ mask, and have collected the results in Table IX. The comparison of Tables VIII and IX shows quantitatively the reduction of the level of Gaussianity for the case of CMB masked maps.

[1] V. Acquaviva, N. Bartolo, S. Matarrese, and A. Riotto, Nucl. Phys. **B667**, 119 (2003); J. Maldacena, J. High Energy Phys. 05 (2003) 013; M. Liguori, F. K. Hansen, E. Komatsu, S. Matarrese, and A. Riotto, Phys. Rev. D **73**, 043505 (2006).

[2] N. Bartolo, E. Komatsu, S. Matarrese, and A. Riotto, Phys. Rep. **402**, 103 (2004).

[3] E. Komatsu *et al.*, arXiv:0902.4759v4.

[4] B. A. Bassett, S. Tsujikawa, and D. Wands, Rev. Mod. Phys. **78**, 537 (2006); A. Linde, Lect. Notes Phys. **738**, 1 (2008).

[5] K. Koyama, S. Mizuno, F. Vernizzi, and D. Wands, J. Cosmol. Astropart. Phys. 11 (2007) 024; E. I. Buchbinder, J. Khoury, and B. A. Ovrut, Phys. Rev. Lett. **100**, 171302 (2008); J.-L. Lehners and P. J. Steinhardt, Phys. Rev. D **77**, 063533 (2008); Y.-F. Cai, W. Xue, R. Brandenberger, and X. Zhang, J. Cosmol. Astropart. Phys. 05 (2009) 011; Y.-F. Cai, W. Xue, R. Brandenberger, and X. Zhang, J. Cosmol. Astropart. Phys. 06 (2009) 037.

[6] L.-Y. Chiang, P. D. Naselsky, O. V. Verkhodanov, and M. J. Way, Astrophys. J. **590**, L65 (2003).

[7] P. D. Naselsky, L.-Y. Chiang, I. D. Novikov, and O. V. Verkhodanov, Int. J. Mod. Phys. D **14**, 1273 (2005).

[8] P. Cabella, D. Pietrobon, M. Veneziani, A. Balbi, R. Crittenden, G. de Gasperis, C. Quercellini, and N. Vittorio, arXiv:0910.4362.

[9] E. Komatsu *et al.*, Astrophys. J. Suppl. Ser. **148**, 119 (2003); D. N. Spergel *et al.*, Astrophys. J. Suppl. Ser. **170**, 377 (2007); E. Komatsu *et al.*, Astrophys. J. Suppl. Ser. **180**, 330 (2009); P. Vielva, E. Martínez-González, R. B. Barreiro, J. L. Sanz, and L. Cayón, Astrophys. J. **609**, 22 (2004); M. Cruz, E. Martínez-González, P. Vielva, and L. Cayón, Mon. Not. R. Astron. Soc. **356**, 29 (2005); M. Cruz, L. Cayón, E. Martínez-González, P. Vielva, and J. Jin, Astrophys. J. **655**, 11 (2007); L. Cayón, J. Jin, and A. Treaster, Mon. Not. R. Astron. Soc. **362**, 826 (2005); Lung-Y Chiang and P. D. Naselsky, Int. J. Mod. Phys. D **15**, 1283 (2006); J. D. McEwen, M. P. Hobson, A. N. Lasenby, and D. J. Mortlock, Mon. Not. R. Astron. Soc. **371**, L50 (2006); J. D. McEwen, M. P. Hobson, A. N. Lasenby, and D. J. Mortlock, Mon. Not. R. Astron. Soc. **388**, 659 (2008); A. Bernui, C. Tsallis, and T. Villela, Europhys. Lett. **78**, 19 001 (2007); L.-Y. Chiang, P. D. Naselsky, and P. Coles, Astrophys. J. **664**, 8 (2007); C.-G. Park, Mon. Not. R. Astron. Soc. **349**, 313 (2004); H. K. Eriksen, D. I. Novikov, P. B. Lilje, A. J. Banday, and K. M. Górski, Astrophys. J. **612**, 64 (2004); M. Cruz, M. Tucci, E. Martínez-González, and P. Vielva, Mon. Not. R. Astron. Soc. **369**, 57 (2006); M. Cruz, N. Turok, P. Vielva, E. Martínez-González, and M. Hobson, Science **318**, 1612 (2007); P. Mukherjee and Y. Wang, Astrophys. J. **613**, 51 (2004); D. Pietrobon, P. Cabella, A. Balbi, G. de Gasperis, and N. Vittorio, Mon. Not. R. Astron. Soc. **396**, 1682 (2009); D. Pietrobon, P. Cabella, A. Balbi, R. Crittenden, G. de Gasperis, and N. Vittorio, Mon. Not. R. Astron. Soc. **402**, L34 (2010); Y. Ayaita, M. Weber, and C. Wetterich, Phys. Rev. D **81**, 023507 (2010); P. Vielva and J. L. Sanz, Mon. Not. R. Astron. Soc. **397**, 837 (2009); B. Lew, J. Cosmol. Astropart. Phys. 08 (2008) 017; A. Bernui and M. J. Rebouças, Int. J. Mod. Phys. A **24**, 1664 (2009); M. Kawasaki, K. Nakayama, T. Sekiguchi, T. Suyama, and F. Takahashi, J. Cosmol. Astropart. Phys. 11 (2008) 019; M. Kawasaki, K. Nakayama, and F. Takahashi, J. Cosmol. Astropart. Phys. 01 (2009) 026; M. Kawasaki, K. Nakayama, T. Sekiguchi, T. Suyama, and F. Takahashi, J. Cosmol. Astropart. Phys. 01 (2009) 042; M. Cruz, E. Martínez-González, and P. Vielva, arXiv:0901.1986.

[10] E. Martínez-González, arXiv:0805.4157; Y. Wiaux, P. Vielva, E. Martínez-González, and P. Vandergheynst, Phys. Rev. Lett. **96**, 151303 (2006); L. R. Abramo, A. Bernui, I. S. Ferreira, T. Villela, and C. A. Wuensche, Phys. Rev. D **74**, 063506 (2006); P. Vielva, Y. Wiaux, E. Martínez-González, and P. Vandergheynst, New Astron. Rev. **50**, 880 (2006); Mon. Not. R. Astron. Soc. **381**, 932 (2007); C. J. Copi, D. Huterer, D. J. Schwarz, and G. D. Starkman, Phys. Rev. D **75**, 023507 (2007); Mon. Not. R. Astron. Soc. **399**, 295 (2009); K. Land and J. Magueijo, Mon. Not. R. Astron. Soc. **378**, 153 (2007); B. Lew, J. Cosmol. Astropart. Phys. 09 (2008) 023; A. Bernui, Phys. Rev. D **78**, 063531 (2008); **80**, 123010 (2009); P. K. Samal, R. Saha, P. Jain, and J. P. Ralston, Mon. Not. R. Astron. Soc. **385**, 1718 (2008); **396**, 511 (2009); A. Bernui, B. Mota, M. J. Rebouças, and R. Tavakol, Astron. Astrophys. **464**, 479 (2007); Int. J. Mod. Phys. D **16**, 411 (2007); T. Kahniashvili, G. Lavrelashvili, and B. Ratra, Phys. Rev. D **78**, 063012 (2008); L. R. Abramo, A. Bernui, and T. S. Pereira, J. Cosmol. Astropart. Phys. 12 (2009) 013; F. K. Hansen, A. J. Banday, K. M. Górski, H. K. Eriksen, and P. B. Lilje, Astrophys. J. **704**, 1448 (2009).

[11] A. Bernui and M. J. Rebouças, Phys. Rev. D **79**, 063528 (2009).

[12] G. Hinshaw *et al.*, Astrophys. J. Suppl. Ser. **180**, 225 (2009).

[13] J. Kim, P. Naselsky, and P. R. Christensen, Phys. Rev. D **77**, 103002 (2008).

[14] J. Delabrouille *et al.*, Astron. Astrophys. **493**, 835 (2009).

[15] B. Gold *et al.*, arXiv:1001.4555.

[16] C. L. Bennett *et al.*, Astrophys. J. Suppl. Ser. **148**, 1 (2003).

[17] G. Hinshaw *et al.*, Astrophys. J. Suppl. Ser. **170**, 288 (2007).

[18] http://lambda.gsfc.nasa.gov/product/map/dr3/ilc_map_get.cfm; http://www.nbi.dk/~jkim/hilc/; and http://www.apc.univ-paris7.fr/APC_CS/Recherche/Adamis/cmb_wmap-en.php.

[19] K. M. Górski, E. Hivon, A. J. Banday, B. D. Wandelt, F. K. Hansen, M. Reinecke, and M. Bartelman, Astrophys. J. **622**, 759 (2005).